Monitoring of the pH Evolution at a Cathodically Protected Steel Surface Subject to an AC Voltage Perturbation

Andreas Junker, M.Sc., Eng.
MetriCorr, Toerringvej 7, 2610 Roedovre, Denmark

Lars Vendelbo Nielsen, Ph.D., Eng.
MetriCorr, Toerringvej 7, 2610 Roedovre, Denmark

Abstract

Assessing AC corrosion with respect to an E-pH or Pourbaix diagram is widely done in literature. No common agreement on the influence of pH on the AC corrosion rate exists however. This paper presents a literature review of the effect of pH on AC corrosion, as well as an in situ investigation of pH and potential of a steel surface at different cathodic protection levels and different AC potential levels. The results are directly correlated to AC corrosion rates measured by the ER technique and discussed in relation to the current EN15280:2013 standard. Furthermore, the effect of faradaic rectification of AC currents on the pH evolution at an electrode surface is illustrated by a novel visualisation experiment.

Introduction

The mechanism of AC corrosion of cathodically protected structures is heavily debated. One factor that remains subject to debate is the effect of pH. The general understanding of cathodic protection involves the formation of a passive layer on steel due to elevated pH or bringing the steel to the immune region in the Pourbaix diagram (Figure 1) by lowering the potential [1] [2]. In either case, under cathodic protection, the cathode reaction creates alkalinity, either by hydrogen evolution (1) or oxygen reduction (2) in acidic or neutral to alkaline environments respectively, or by dissociation of water under anaerobic conditions (3).

$$2H^+ + 2e^- \rightarrow H_2(g) \quad (1)$$

$$O_2 + 2H_2O + 4e^- \rightarrow 4OH^- \quad (2)$$

$$2H_2O + 2e^- \rightarrow H_2(g) + 2OH^- \quad (3)$$

With respect to AC corrosion the typical scenario is cathodic protection of buried pipelines. Here, the natural oxygen content and acidity in the soil will be depleted and with time reaction (3) will be the governing reaction [1]. The produced hydroxyl-ions increase the ionic conductivity of the soil, which leads to a reduction of the spread resistance and consequently increased AC and DC current densities at static AC and DC voltages [3] [4] [5] [6]. This is an autocatalytic process since increased DC current densities enhances the cathode reactions and hence the ionic conductivity and alkalisation etc. Adversely, an increased pH also alters the solubility of different species in soil. In particular the earth alkaline elements (mostly Ca and Mg) can precipitate as carbonates or hydroxides in high pH environments as species of very low solubility [7]. Calcareous deposits on a steel surface will increase the spread resistance and limit AC corrosion [8], however the effect of passing AC currents and hydrogen evolution from reaction (3) may be detrimental to the mechanical stability of these deposits, resulting in a dynamic AC corrosion mechanism with continuous build-up and break-down of the formed deposit [4]. The presence of alkaline and earth alkaline ions in solution may also act as an inhibitor for pH increase, since these will consume formed OH^- upon formation of solid hydroxides [9]. The pH buffering capabilities of the carbonate/bicarbonate system naturally occurring in many soils may also hinder the immediate pH increase until the bicarbonate is converted to carbonate [10].

In Figure 1 the Pourbaix diagram for steel is shown. It is calculated using the HSC E-pH Chemistry software at 25°C and 1 bar pressure and takes into account the effect of concentration of different Fe species in solution from 10^0 – 10^{-6} mol/l. The present diagram favours the formation of the iron oxides Fe_2O_3 and Fe_3O_4. It can be seen that an elevated pH contributes to passivating the steel within the stability region of water between the stippled lines, while a too high pH may cause the steel to enter the high pH $HFeO_2^-$ corrosive region. The pH limits for entering this region are generally believed to be very high at pH > 13-14 [2],

but as the calculated example in Figure 1 shows, this limit is highly dependent on the concentration of iron in solution. This is often neglected in most literature on high pH corrosion. The strong dependency on the concentration of dissolved iron species must also be considered in the case of AC corrosion, where iron dissolution and the resulting increase in concentration may cause this region to shrink, unless the dissolved iron is immediately consumed by reactions with species in the electrolyte forming e.g. corrosion products.

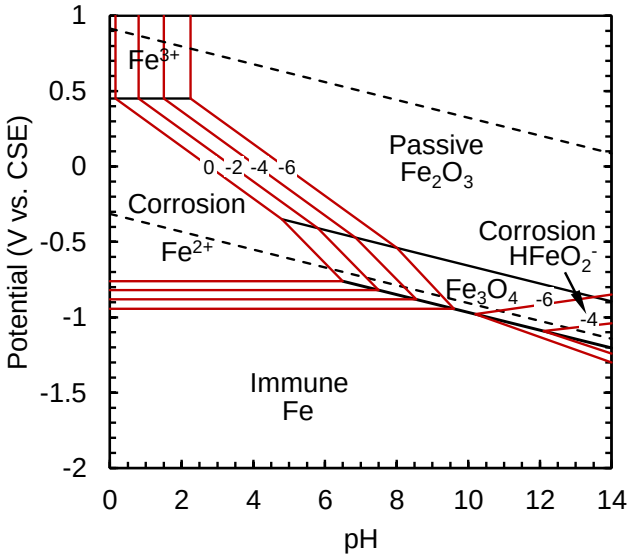

Figure 1: Calculated Pourbaix diagram for 25°C and 1 bar pressure. The corrosive regions are highly dependent on the concentration of Fe in solution indicated by the log([Fe]) values.

Nielsen et.al. presented an alkalisation theory associated with an incubation period before the pH would reach a critical level and AC corrosion rates would dramatically increase. The authors linked this effect to reaching the high pH corrosion region in the Pourbaix diagram. The incubation period is a function of the OH^- neutralising capacity of different soils, and depending on the soil, this incubation period may be several weeks [11].

Using a retractable pH electrode, Brenna et.al. measured a pH profile in the proximity of a carbon steel surface under cathodic protection at different DC current densities (0.5-7A/m^2) [12]. This is shown in Figure 2a. They found that the major pH increase occurs within the first 2 mm from the electrode surface. With higher cathodic current, the higher the pH maxima at the electrode (pH = 12-13.5) and the further the high pH region extends into the electrolyte. The effect of time is however unclear from the study. The suggested corrosion mechanism by Brenna et.al. [13] is an electromechanical breakdown mechanism of the passive film on cathodically protected steel caused by high alternating voltages, followed by an aggressive increase of pH in the formed cracks where chemical corrosion as $HFeO_2^-$ is possible according to the Pourbaix diagram.

A similar strong dependence on the distance from the steel surface on the pH is reported by Gummow et.al. [14]. They report a pH increase within the first few mm of several pH values, but also take into account the pH of the bulk solution which has a high influence of the maximum obtainable pH value at the steel surface at a fixed DC current density of 0.38A/m^2.

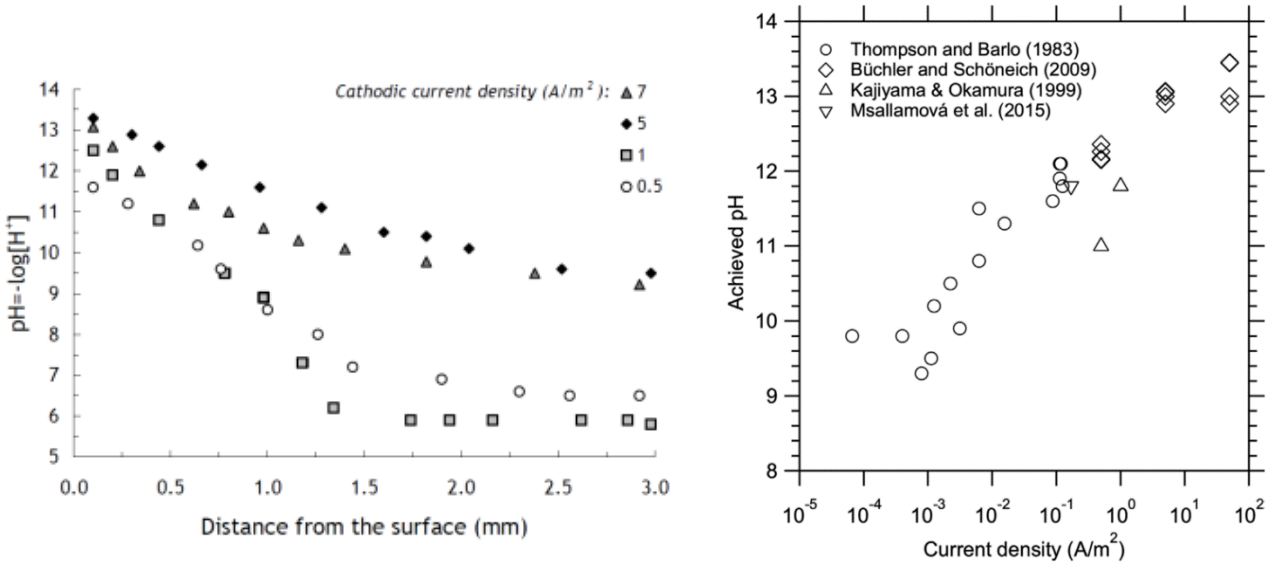

a) pH profiles for varying CP current density. No AC applied. Notice the large variation with the distance from the surface [12].

b) Current density dependency on the achievable pH under cathodic protection. No AC applied. Notice the almost linear dependency [1].

Figure 2: Investigations of the effect of the DC current density on the pH at a steel surface found in literature.

Based on the findings by Thompson and Barlo [15] and Büchler and Schöneich [16] shown in Figure 2b, Büchler and Joos [3] developed an expression for the pH as a function of the DC current density shown in (4).

$$pH = pH_0 + p \cdot \log(J_{DC}) \quad (4)$$

They found optimized parameters for $pH_0 = 12.4$ and $p = 0.5$ and developed an empirical model that makes it possible to determine the influence of pH on the local soil resistivity and spread resistance. Surely factors such as the soils' OH^- neutralising capacity, local diffusion coefficients for the reacting species in (3) and possible convection of the solution etc. affects the developing pH and complicates this simple empirical regression, but it offers a nice understanding of the direct relationship between the current density, i.e. the amount of electrons participating in cathode reaction (3) and the amount of OH^- ions being produced at the same surface, refer the general equation for pH as a function of $[OH^-]$ given in (4).

$$pH = 14 + \log([OH^-]) \quad (4)$$

With the pH being a relatively simple function of the applied DC current density, controlling the pH should be a relatively straight forward procedure. However, the polarisation behaviour of a steel is heavily influenced by the AC current density, and the obtained DC current densities can be enhanced by orders of magnitude due to faradaic rectification of the AC current. Faradaic rectification is mathematically well described by several authors [17] [18] [19] [20] [21], and documented effects of this phenomenon are reported by several authors whether it is described as a 'depolarisation effect', an 'increased exchange current effect' or as faradaic rectification [5] [22] [23] [24] [25]. In conclusion; high DC current densities and the following alkalisation may be difficult to avoid in the special case of AC interference and AC corrosion.

In an attempt to focus the investigation on the influence of pH on AC corrosion, Tang and Du et.al. designed an experiment with fixed pH solutions at pH = 6.4, 10, 11, 12 and 13, as an alternative to cathodic protection [26]. They then subjected carbon steel samples to various AC current densities (0-300 A/m^2) and found that corrosion rate measured by weight-loss was proportional to the AC current density, but inversely proportional to the pH, which they attributed to passivation of the steel at high pH. This investigation however, fails to take into account that 1) pH = 13 may in fact be too low to enter the high pH corrosion region in the Pourbaix diagram. 2) The polarisation of the steel caused by cathodic protection puts the steel in a whole different place in the Pourbaix diagram. 3) The present experiment is static in terms of pH and AC current density, whereas the cathode reaction is known to contribute to the evolution of both the pH and the spread resistance, positive or negative depending on the chemical environment, and thus the AC current density. This is in line with the conclusion by Büchler and Schöneich who made a similar experiment in a pH = 14 solution at very high AC current densities (500-1200 A/m^2), but found that even under these conditions no significant corrosion was observed [16]. This suggests that a high pH alone in combination with an AC current is not sufficient to induce AC corrosion.

A alternative theory on the effect of pH on AC corrosion was hypothesized by Tribollet and Meyer et.al upon the observation of an intermediate green rust corrosion product ($[Fe^{II}_{1-x}Fe^{III}_x(OH)_2]^{x+}[x/nA^{n-}m/nH_2O]^{x-}$) on a cathodically protected steel subject to an AC perturbation. This green rust is however only stable at pH values < 11, and the stability of this phase may be linked to maintaining a protective layer, even under AC perturbation [27]. This can easily be linked to Büchlers hypothesis that corrosion products covering the surface may be able to accommodate the alternating charge via a pseudo capacitance caused by continuous oxidation/reduction of Fe^{2+}/Fe^{3+} ions in the surface film rather than at the steel surface [16] [28]. In fact such a mechanism is described by Antony et.al. for green rust films [29], but the films are usually not stable and will oxidize to α- or γ-FeOOH, Fe_2O_3 or Fe_3O_4 with alternative ageing processes [30] [31], in good accordance with the analysis of corrosion products in AC corrosion cases [32] [33]. Tribollet and Meyer list two possible routes to destabilisation of the green rust phase, both triggered by high pH caused by the water reduction reaction (3): Excessive CP or faradaic rectification of high alternating currents.

Methods

Visualisation of the alkalisation

Visualisation of the alkalisation at a probe surface is done by making a transparent soil simulation with added phenolphthalein pH indicator. Commercially available 'water beads' made from superabsorbent polymer were soaked in a non-scaling artificial soil simulation (**Error! Reference source not found.**), causing them to swell from 1.9 mm to 10 mm diameter spheres. Consisting of ~99% solution they have approximately the same refractive index as the solution, and are thus transparent in this solution. By blending the swelled beads to a slurry, a fine grained solution is obtained. This slurry is transparent but in terms of grain structure and diffusion properties, it is estimated that it resembles a wetted sand solution, thus allowing for a visualisation of the alkalisation at an electrode by observing the change of colour of the pH indicator.

Table 1: Non-scalin artificial soil solution used in the experiments

Species	Concentration
Na_2SO_4	$5.0 \cdot 10^{-3}$ M
$NaHCO_3$	$2.5 \cdot 10^{-3}$ M
NaCl	$10.0 \cdot 10^{-3}$ M

The slurry of blended water beads and solution is put in a rectangular glass container to minimize the visual distortion of the image, and a 10:1 length/width-ratio, 1 cm^2 working electrode is placed in the field of view of a camera outside the container (Figure 3). Two counter electrodes are placed in either side of the container and connected to the working electrode via an AC generator and a 600 µF capacitor on one side, and a DC potentiostat and a 3H inductor on the other side to filter out AC on the potentiostat and DC on the AC generator. A thin oil film on top of the solution is added to hinder evaporation of the solution. A 100 mV stepwise increase of the cathodic protection level from -950 mV to -1250 mV (CSE) is applied to the coupon over a period of 11 days and the experiment is repeated two times; once without AC and once with a 10 V AC perturbation. The camera is set to take an image every minute, in order to produce an illustrative fast forward time-lapse video of the pH evolution.

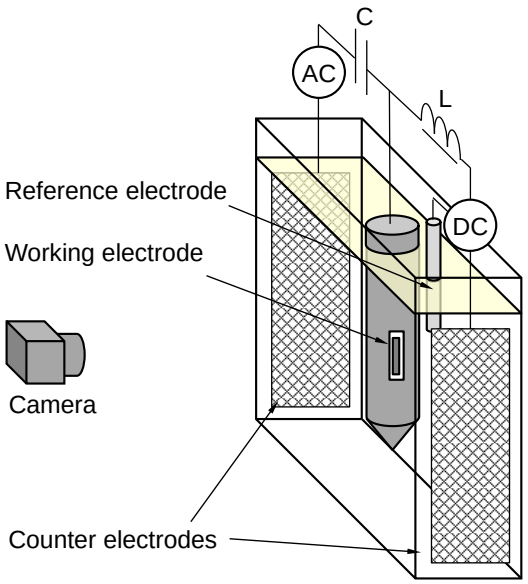

Figure 3: Experimental setup for visualisation of pH evolution at an electrode under AC and DC influence. The electrolyte is a transparent slurry simulating wetted sand, containing a phenolphthalein pH indicator with a transparent to pink colour change at pH > ~9.

pH monitoring

To monitor the pH at a cathodically protected steel surface under AC perturbation, a dedicated experimental cell was designed. This setup can be seen in Figure 4. A 10:1 length/width-ratio, 1 cm^2 ER probe was used as the working electrode in an identical electrical circuit to that of the visualisation experiment with a separation of the AC and DC circuit. The cell was filled with sand (0.4-0.8 mm) and wetted with a non-scaling artificial soil solution given by **Error! Reference source not found.**. The resulting soil resistivity was ~18.5 Ωm. A pH electrode with a tip diameter of 3 mm and a small temperature electrode was placed ~5 mm from the probe surface. This distance was chosen to avoid disturbing the electrode surface during the experiment. A reference temperature electrode not shown in Figure 4 was placed in “remote earth” in the setup to be able to monitor the temperature increase at the surface and compensate for daily temperature variations. The temperature was recorded every 10 minutes by a Grant Squirrel data logger. The ER probe measured electrical parameters E_{on}, $E_{IR\text{-}free}$, U_{AC}, J_{DC}, J_{AC}, R_S and probe element thickness, d, every 15 minutes during the experimental period of 6 days. The pH was read manually from a pH

meter. During the first hour of the experiment where the pH increase was particularly pronounced, the pH-measurement frequency was high (every minute).

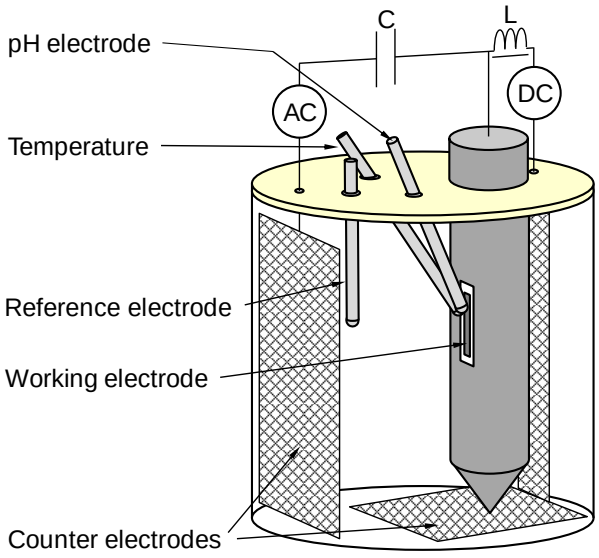

Figure 4: Experimental setup for monitoring of pH evolution at an electrode under AC and DC influence.

The pH monitoring experiment was repeated three times with different potentiostatic AC and DC voltage conditions. The reason for running the experiments potentiostatically was to monitor the influence of these settings on the pH, and vice versa; the influence of the developing pH on the electrical parameters such as the spread resistance and current densities. Each experimental run was labelled I-III according to Table 2. Experiment I and II represents a cathodically protected pipeline with or without AC, allowing for a direct assessment of the effect of AC on the developing pH in front of a coating defect. Experiment II and III represents a pipeline under AC interference, but they allow for an assessment of the effect of having a medium or high CP level.

Table 2: Experimental matrix for different AC and DC voltage conditions

Experiment	Eon (mV vs. CSE)	U_{AC} (V_{RMS})
I	-1200	0
II	-1200	10
III	-1550	10

Results

Visualisation of the alkalisation

The result of the pH visualisation experiment is illustrated in Figure 5. Daily still images show a progressive change in the local pH environment and the main findings are listed below:

- The pink colouration, i.e. a pH > 9 environment, is far more pronounced for the 10 V AC experiment. For both experiments the Eon potential has a large influence on the evolving environment. Time is clearly also an influential factor in terms of the extent of the high pH environment, however difficult to evaluate properly for the relatively short term experiment.

- The experiment does not offer any information about a pH gradient field towards the electrode, i.e. the pH within the pink area may be much higher than 9.
- The DC current density is increased by the presence of AC by almost one order of magnitude. This is a direct effect of faradaic rectification of the AC current.
- Gas evolution at the electrode surface causes an upwards drift of the high pH environment for the 10 V AC experiment via a 'pump effect' of the upwards drifting gas bubbles. This is attributed to the high DC current that surpasses the hydrogen overvoltage. At -1250 mV the DC current for the 0 V AC experiment is just enough to produce hydrogen gas showing a small upwards tail of the pink pH environment.
- The alkalisation at the electrode not affected by AC appears very localised.
- No corrosion was recorded in either experiment with or without AC.

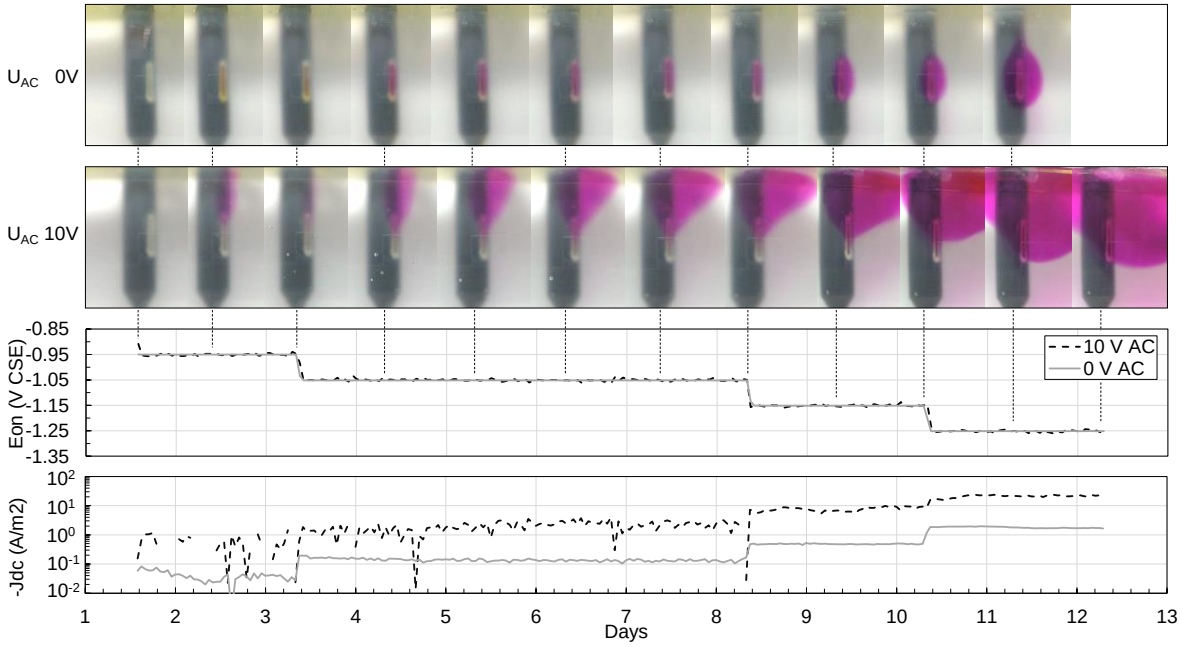

Figure 5: Visualisation of the an evolving pH > 9 environment in front of a steel surface at increasingly negative potentials from -950 mV to -1250 mV (CSE) with or without an AC perturbation. The higher DC current, caused by faradaic rectification of the AC current, is directly related to the cathode reaction and OH^- development.

pH monitoring

The results from the pH monitoring experiment are presented in Figure 6 for the three different experimental conditions I-III (Table 2). In Figure 6a the measured pH (5 mm) shows a rapid increase in the beginning of each experiment, after which it stabilises on a level that is highly dependent on the AC and DC voltage conditions. On the same plot, a series of calculated pH values are shown based on the recorded DC current densities and equation (4). It can be seen that these values are approximately 1 pH value higher. Taking into account that equation (4) calculates the pH at the probe surface (0 mm) it is very plausible that a pH increase towards the surface may be responsible for this discrepancy. Based on work by other authors, e.g. Figure 2a, a 1 pH value difference may even be conservative [12] [14]. Taking into account the good correlation; $pH_{calc.} = pH_{meas.} + 1$ for all three experimental conditions, equation (4) is assumed to yield a valid approximation to the actual surface pH, also in this work.

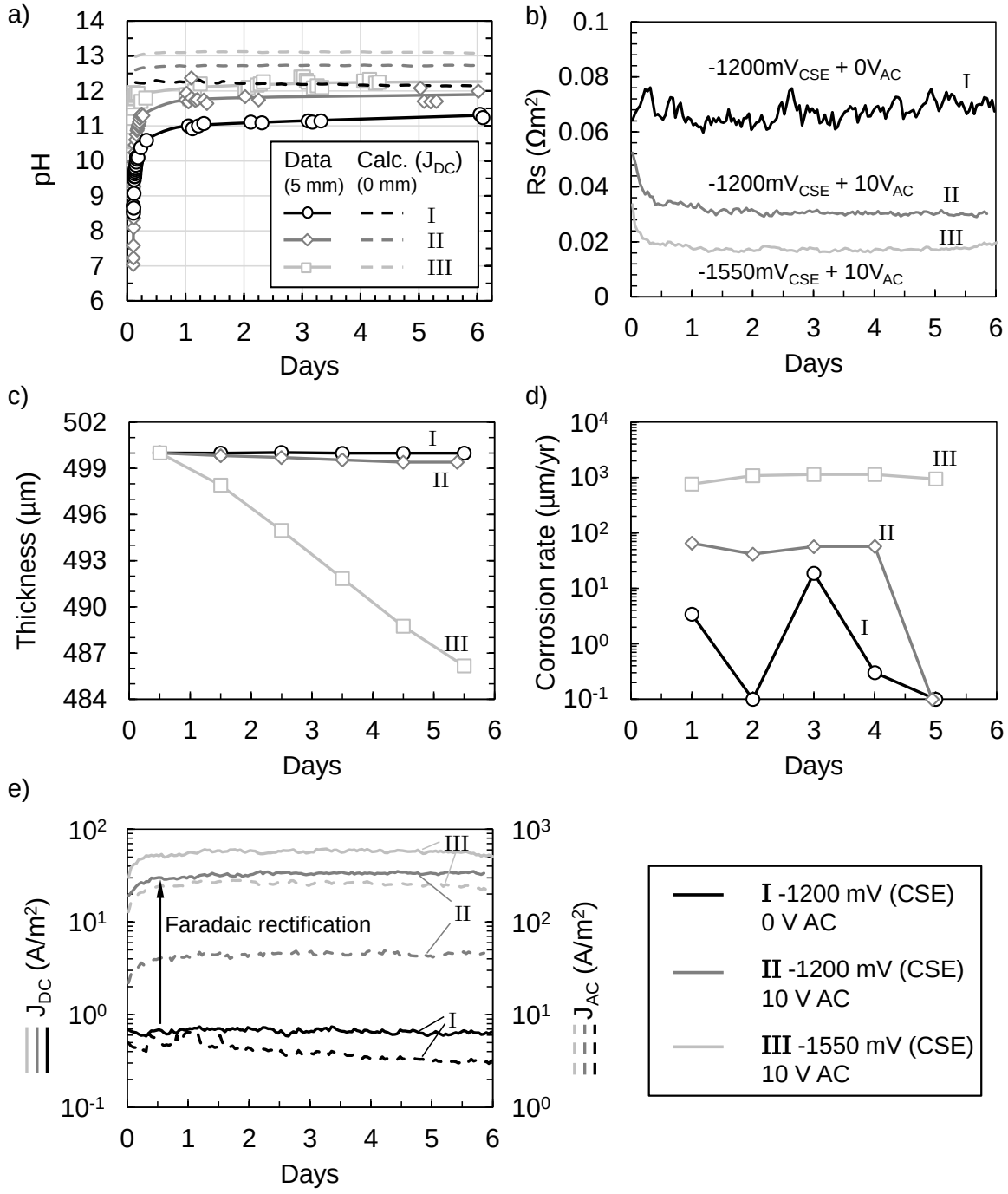

Figure 6: Data for the various experiments (I, II and III) as a function of time.
a) pH as measured 5 mm from the surface and calculated at 0 mm by means of the current density (4) yielding approx. +1 in pH.
b) The evolution in spread resistance, R_S
c) Thickness (daily averages)
d) Corrosion rate (daily averages).
e) Both AC and DC current densities plotted as stippled and solid lines respectively. The effect of faradaic rectification is clear when comparing experiment I and II having the same on-potential of -1200 mV (CSE)

In Figure 6b the corresponding spread resistance is shown. The effect of pH on this value will be further elaborated on in the discussion. In Figure 6c and d, daily averaged thickness and calculated corrosion rates are shown. The corrosion rate can be seen to increase by approximately one order of magnitude from experiment I to II and from II to III. The large scatter of I is partially due to the logarithmic scale but all corrosion rates here were < 20 µm/yr. Towards the end of experiment II the corrosion rate decreased, however the reason for this is unknown. Figure 6e shows both the DC and AC current densities, and the faradaic rectification of the AC current is clear from the large increase of J_{DC} from experiment I to II having the same Eon potential. A small AC signal (~0.4 V) was applied to the I-experiment to allow for spread resistance calculation by the data logger, however this can be seen to be only 3-6 A/m^2, i.e. far below the AC current density threshold of 30 A/m^2 given by the EN15280:2013 standard, and thus not of concern with respect to AC corrosion. The DC current density of the I-experiment is also below the limit of < 1 A/m2 given by the EN15280:2013 standard and the low corrosion rates confirm the effective CP. Comparing current densities from the II and III experiment, it can be seen that not only does the DC current density increase with a higher degree of cathodic polarisation, but so does the AC current density. This is related to the increased alkalisation following the enhanced cathode reaction that lowers the spread resistance and causes a higher AC current density at the same alternating voltage.

The temperature at the 5 mm distance to the electrode surface was measured during the experiment, and the difference compared to the surrounding solution was calculated as ΔT (°C) = T_{5mm} - T_{remote}. This is plotted in Figure 7a. The temperature increase is caused by joule heating of the probe surface caused by the passing AC currents as can be seen in Figure 7b where average ΔT and J_{AC} values are plotted. This is in line with results obtained by Nielsen [34], and the limited temperature increase observed may be ignored in terms of pH correction.

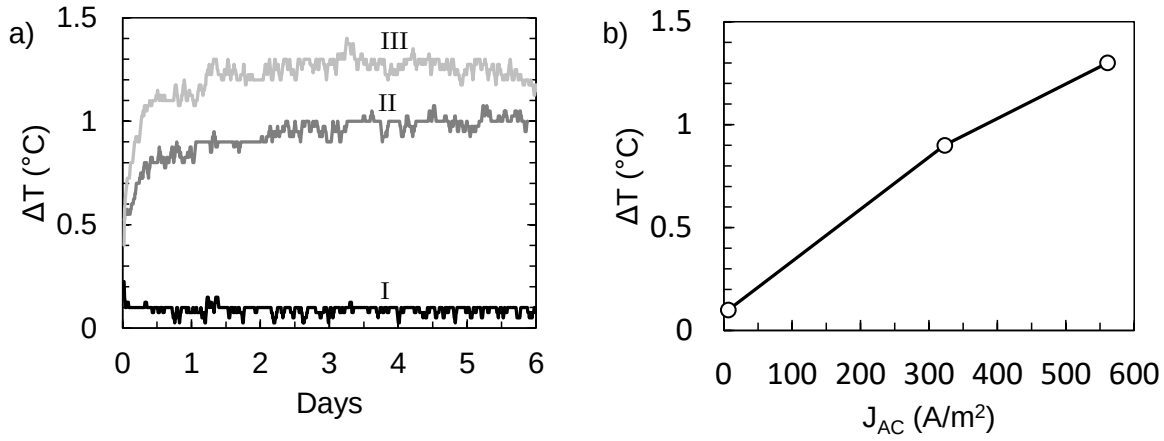

Figure 7: Temperature monitoring of the probe surface (5 mm) showing a negligible temperature change as a function of J_{AC}.

Discussion

This work investigates the effect of pH on AC corrosion of cathodically protected steel. One thing that may be concluded is that the increase in pH is linked to an increase in the ionic conductivity of the soil locally around a coating defect, and thus a decrease of the spread resistance. This is not new knowledge but confirms accepted theory, refer the introduction. In Figure 8 the measured spread resistance from the ER probe in the pH monitoring experiment is shown as a function of the measured pH values 5 mm from the probe surface

and the calculated pH values at the surface (0 mm). The trend is a linear decrease of spread resistance with pH. These results are valid for the non-scaling artificial soil used in the present investigation having a soil resistivity of ~18.5 Ωm, and the correlation may be different for other soils. Since it is generally accepted that corrosion rate is a function of the AC current density (even in the absence of DC current) this is part of the explanation for the great dependence on the DC current density. Increased AC current density on a cathodically protected structure is a direct consequence of the alkalisation caused by the cathode reactions. That is, unless the alkalisation causes precipitation of calcareous deposits that increase the spread resistance.

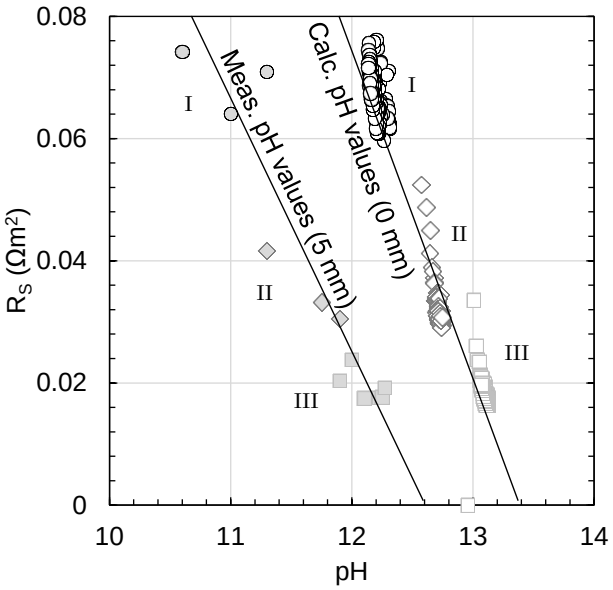

Figure 8: The effect of pH on the spread resistance caused by an increase of the ionic conductivity at the probe surface. Results from the measured pH values (trend line) as well as calculated pH values based on the DC current density and equation (4).

If the calculated pH values at the steel surface can be accepted as true, then these may be used together with the IR-free polarised potential measured by the ER probe to map out in which stability region in the Pourbaix diagram a steel surface exists. This has been done in Figure 9 for daily averaged values, and each point has been plotted as a circle whose size and colour corresponds to a corrosion rate. This representation puts the I-experiment in the immune region of the diagram as low/no corrosion points corresponding to effective CP. In case of an AC perturbation (II and III), the hydrogen evolution cathode reaction (3) becomes enhanced by faradaic rectification of the AC current, as was also verified by the visualisation experiment, and the points fall exactly on the hydrogen line. This is remarkable since it is perfectly in line with the theory that the potential of a steel is shifted parallel to the hydrogen line towards higher pH under cathodic protection [28], and this may further verify that the calculated pH values are representative of the true pH at the surface. Observing the stability region of various species in the Pourbaix diagram it can be seen that the III-experiment falls within the log([$HFeO_2^-$]) = -4 region (much dependent on the concentration of iron species). This may be interpreted as an argument for high pH chemical corrosion being the corrosion mechanism in play, however; the present calculated stability region differ significantly from that of the vast majority of literature (that starts at pH = 13-14, but is often ignoring the effect of the concentration of the iron containing species). With high corrosion rates this region would quickly be expected to shrink towards very high pH. Since AC

corrosion is not slowing down after a period of corrosion (and increasing iron species concentration) this implies either that $HFeO_2^-$ is quickly being converted to stable oxides, e.g. during the anodic half-wave of the AC cycle, or that high pH chemical corrosion is in fact an unlikely AC corrosion mechanism.

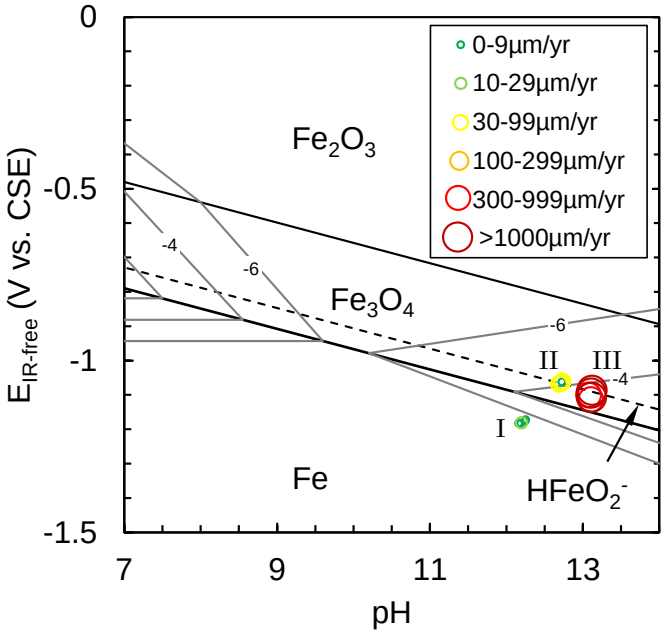

Figure 9: Corrosion rates plotted as points in the Pourbaix diagram at the corresponding calculated pH and measured EIR-free value. High corrosion rates fall within the $HFeO_2^-$ stability region. Without AC, the steel is in the immune region and no corrosion is measured.

The effects of faradaic rectification of AC currents and enhancement of the cathode reaction (3) are two-fold: alkalisation is strongly enhanced and hydrogen evolution occurs at high rates. The visualisation experiment clearly showed the great influence of an AC perturbation on steel at increasingly negative cathodic polarisation. The missing corrosion in the visualisation experiment may perhaps be explained by a continuous removal of the high pH environment at the surface via the hydrogen 'pump effect', due to a too low viscosity of the transparent soil simulation compared to real soil.

While most literature links AC corrosion to elevated pH and high AC and DC current densities, the hydrogen evolution is rarely considered to take part in the corrosion mechanism, except for perhaps destabilising surface deposits [4]. Following the different studies conducted in high pH solutions with high AC current densities that yielded little to no corrosion [16] [26], it is interesting that the only part missing from the real case is the negative polarisation and the hydrogen evolution at the surface. Both pH and J_{DC} can be interpreted as a measure of produced hydrogen as well. When observing the visualisation experiment in the present study however, plenty of hydrogen was produced at a surface with both an AC and DC current density influence above the limits given by the EN15280:2013 standard, while no corrosion was observed. Undoubtedly AC corrosion is influenced by several processes, making the mechanism particularly complicated.

Conclusion

The pH at a cathodically protected surface is dependent on both the DC polarisation, as well as an alternating current. This has been shown both in a novel visualisation experiment and by direct monitoring of the pH using a small pH electrode in front of a surface.

The high pH environment in front of a coating defect was visually shown to increase in size with increasing polarisation and DC current under pure CP conditions, but when 10 V AC was applied in addition to the same CP conditions, the DC current increased by an order of magnitude by faradaic rectification of the AC current and the high pH environment was increased several factors in size. Excessive hydrogen evolution was observed as a result of the increase in cathodic current.

In another experiment the pH was likewise found to be increasing with both an overlying AC perturbation by faradaic rectification, and by increased cathodic polarisation. The spread resistance decreases due to an increase in ionic conductivity of the increasingly alkaline environment which causes increased AC and DC current densities, and ultimately increased AC corrosion rates.

A satisfying correlation between measured pH values and pH values calculated from the DC current density was obtained. Plotting corrosion rates measured by ER probe in a Pourbaix diagram at calculated pH and $E_{IR\text{-}free}$ positions showed that high pH chemical corrosion as $HFeO_2^-$ may be a possible corrosion mechanism, but this implies that any formed $HFeO_2^-$ must immediately be converted to stable iron oxides. The present investigation remains inconclusive on this particular matter.

Future work

The experimental setups used in this study have proven as powerful remedies to study the evolving pH environment at a coating defect under combined AC and DC influence, and hopefully future experiments in these setups will continue to bring forward new findings on AC corrosion. In particular three factors will be investigated further:

- The effect of extended time studies. I.e. the coupling of an incubation period of perhaps several weeks to the developing pH environment at an electrode.
- A 3 mm pH electrode was used in the present study at a distance of 5 mm to the probe surface. The use of micro electrodes having a measurement tip of < 100µm, placed closer to the surface or moved along a profile may yield a more detailed description of the local pH environment.
- Finite element modelling of the local evolving pH environment based on experimental data may help give a better holistic view of the processes that may/may not take place at the steel surface.

Acknowledgements

This paper was made as part of a research collaboration between MetriCorr and the Technical University of Denmark. The authors would like to thank both for academic support and supply of laboratory equipment. The project is financially supported by the Danish Innovation Fund.

Bibliography

[1] U. Angst, M. Büchler, B. Martin, H.-G. Schöneich, G. Haynes, S. Leeds and F. Kajiyama, “Cathodic protection of soil buried steel pipelines - a critical discussion of protection criteria and threshold values,” *Materials and Corrosion,* vol. 67, no. 11, p. 1135–1142, 2016.

[2] M. Pourbaix, Atlas of Electrochemical Equilibria in Aqueous Solutions, Houston: National Association of Corrosion Engineers, 1974, pp. 307-321.

[3] M. Büchler and D. Joos, “AC-corrosion on cathodically protected pipelines: A discussion of the involved processes and their consequences on mitigation measures,” SGK Swiss Society for Corrosion Protection, Switzerland, 2016.

[4] A. Junker, L. V. Nielsen and P. Møller, “Effect of Chemical Environment and pH on AC Corrosion of Cathodically Protected Structures,” in *NACE Corrosion*, New Orlears, 2017.

[5] M. Büchler, C.-H. Voûte and D. Joos, “Field Investigation of AC Corrosion,” in *CEOCOR*, Menthon-Saint-Bernard, 2011.

[6] L. V. Nielsen, M. B. Petersen, L. Bortels and J. Parlongue, “Effect of Coating Defect Size , Coating Defect Geometry , and Cathodic Polarization on Spread Resistance : - Consequences in relation to AC Corrosion Monitoring,” in *CeoCor*, Bruges, 2010.

[7] F. Stalder, “Influence of alkaline and earth alkaline Cations on the development of the spread resistance of cathodically protected coupons,” CeoCor, 2001.

[8] H. G. Schöneich, “Discussion of criteria to assess the alternating current corrosion risk of cathodically protected pipelines,” Ruhrgas AG, Essen, 2004.

[9] L. V. Nielsen, “pH Gradients Existing in Proximity of Cathodically Charged Steel Buried in Sediment,” Department of Manufacturing Engineering, Materials Technology, Technical University of Denmark, Kgs. Lyngby, DK, 2000.

[10] L. V. Nielsen, “Themodynamic Considerations on the Local Chemistry Formed at the Steel-Soil Interface of Cathodically Protected Pipelines,” Department of Manufacturing Engineering, Materials Technology, Technical University of Denmark, Kgs. Lyngby, DK, 2000.

[11] L. V. Nielsen, B. Baumgarten and P. Cohn, “On-site measurements of AC Induced Corrosion: Effect of AC and DC Parameters,” in *CEOCOR*, Dresden, 2004.

[12] A. Brenna, M. V. Diamanti, L. Lazzari and M. Ormellese, “A proposal of AC corrosion mechanism in cathodic protection,” in *Tech. Proc. of NSTI Nanotechnology Conference and Expo*, Danville, CA, 2011.

[13] A. Brenna, M. Ormellese and L. Lazzari, “Electromechanical Breakdown Mechanism of Passive Film in Alternating Current-Related Corrosion of Carbon Steel Under Cathodic

Protection Condition," *Corrosion,* vol. 72, no. 8, pp. 1055-1063, 2016.

[14] R. A. Gummow, S. Segall and D. Fingas, "An Alternative View of the Cathodic Protection Mechanism on Buried Pipelines," *Materials Performance,* vol. 56, no. 3, pp. 32-37, 2017.

[15] N. G. Thompson and T. J. Barlo, "Fundamental process of cathodically protecting steel pipelines," in *Gas Research Conference, Government Institute*, Rockville, MD, USA, 1983.

[16] M. Büchler and H. G. Schöneich, "Investigation of Alternating Current Corrosion of Cathodically Protected Pipelines: Development of a Detection Method, Mitigation Measures, and a Model for the Mechanism," *Corrosion,* vol. 65, no. 9, pp. 578-586, 2009.

[17] U. Bertocci, "AC Induced Corrosion. The Effect of Alternating Voltage on Electrodes Under Charge Transfer Control," *CORROSION,* vol. 35, no. 5, pp. 211-215, 1979.

[18] S. Lalvani and X. Lin, "A Revised Model for Predicting Corrosion of Materials Induced by Alternating Voltages," *Corrosion Science,* vol. 38, no. 10, pp. 1709-1719, 1996.

[19] R. Bosch and W. Bogaerts, "A Theoretical Study of AC-induced Corrosion Considering Diffusion Phenomena," *Corrosion Science,* vol. 40, no. 2/3, pp. 323-336, 1998.

[20] I. Ibrahim, B. Tribollet, H. Takenouti and M. Meyer, "AC-Induced Corrosion of Underground Steel Pipelines. Faradaic Rectification under Cathodic Protection: I. Theoretical Approach with Negligible Electrolyte Resistance," *J. Braz. Chem. Soc.,* vol. 26, no. 1, pp. 196-208, 2015.

[21] I. Ibrahim, B. Tribollet, H. Takenouti and M. Meyer, "AC-Induced Corrosion of Underground Steel Pipelines. Faradaic Rectification under Cathodic Protection: I. Theoretical Approach with Electrolyte Resistance and Double Layer Capacitance for Bi-Tafelian Corrosion Mechanism," *J. Braz. Chem. Soc.,* vol. 27, no. 3, pp. 605-615, 2016.

[22] S. Goidanich, L. Lazzari and M. Ormellese, "AC Corrosion - Part 1: Effects on overpotentials of anodic and cathodic processes," *Corrosion Science,* vol. 52, no. 2, pp. 491-497, 2010.

[23] S. Giodanich, L. Lazzari and M. Ormellese, "AC Interference Effects on Polarized Steel," p. 12, 2003.

[24] L. V. Nielsen, "Effects of 50 Hz AC on the DC Polarisation Behaviour of Steel Exposed in Artificial Soil Solutions," Department of Manufacturing Engineering, Materials Technology, Technical University of Denmark, Kgs. Lyngby, 2004.

[25] Y. B. Guo, C. Liu, D. G. Wang and S. H. Liu, "Effects of alternating current interference on corrosion of X60 pipeline steel," *Petroleum Science,* vol. 12, no. 2, pp. 316-324, 2015.

[26] D.-Z. Tang, Y.-X. Du, M.-X. Lu, Y. Liang, Z.-T. Jiang and L. Dong, “Effect of pH value on corrosion of carbon steel under an applied alternating current,” *Materials and Corrosion,* vol. 66, no. 12, pp. 1467-1479, 2015.

[27] B. Tribollet and M. Meyer, “Chpt. 2: AC-Induced Corrosion of Underground Pipelines,” in *Underground Pipeline Corrosion*, Woodhead Publishing, 2014, pp. 35-61.

[28] M. Büchler, “Alternating Current Corrosion of Cathodically Protected Pipelines: Discussion of the Involved Processes and their Consequences on the Critical Interference Values,” *Materials and Corrosion,* vol. 63, no. 12, pp. 1181-1187, 2012.

[29] H. Antony, L. Legrand and A. Chaussé, “Carbonate and Sulphate Green Rusts - Mechanisms of Oxidation and Reduction,” *Electrochimica Acta,* vol. 53, no. 24, pp. 7146-7156, 2008.

[30] L. Legrand, L. Mazerolles and A. Chaussé, “The Oxidation of Carbonate Green Rust into Ferric Phases: Solid-state Reaction or Transformation via Solution,” *Geochimica et Cosmochimica Acta,* vol. 68, no. 17, pp. 3497-3507, 2004.

[31] G. Ona-Nguema, M. Abdelmoula, F. Jorand, O. Benali, A. Gehin, J. C. Block and J. M. R. Genin, “Iron(II,III) hydroxycarbonate green rust formation and stabilization from lepidocrocite bioreduction,” *Environmental Science and Tachnology,* vol. 36, no. 1, pp. 16-20, 2002.

[32] F. Stalder and D. Bindschelder, “Wechselstrominduzierte Korrosionsangriffe auf eine Erdgasleitung,” *Gas Wasser Abwasser,* vol. 71, pp. 307-313, 1991.

[33] P. Lindhardt and G. Ball, “AC Corrosion: Results from Laboratory Investigations and from a Failure Analysis,” *CORROSION,* no. 06160, 2006.

[34] L. V. Nielsen, “Possible temperature effects on A.C. Corrosion and A.C. Corrosion Monitoring,” in *CEOCOR*, Brussels, Belgium, 2012.